ISSN 1024-8560, Atmospheric and Oceanic Optics, 2017, Vol. 30, No. 6, pp. 508–516. © Pleiades Publishing, Ltd., 2017.
Original Russian Text © A.V. Konoshonkin, 2017, published in Optika Atmosfery i Okeana.

REMOTE SENSING OF ATMOSPHERE, HYDROSPHERE, AND UNDERLYING SURFACE

Optical Characteristics of Irregular Atmospheric Ice Columns

A. V. Konoshonkin[a, b]

[a] *National Research Tomsk State University, Tomsk, 634050 Russia*
[b] *V.E. Zuev Institute of Atmospheric Optics, Siberian Branch, Russian Academy of Sciences, Tomsk, 634055 Russia*
e-mail: sasha_tvo@iao.ru

Received February 20, 2017

Abstract—The study of cirrus clouds, which significantly affect the climate, is carried out using lidars. Interpretation of the lidar data is based on the direct solution of the problem of light scattering by particles of crystal clouds. Optical characteristics of perfect ice hexagonal columns, obtained previously, poorly agree with the lidar observation results. The work describes calculations of the optical characteristics of irregular hexagonal ice columns, which are in a good agreement with the experimental results. The calculations for particles with deformation of a dihedral angle of 90° are presented. It is shown that the logarithm of the scattering matrix can be linearly approximated well by the logarithm of the particle size. This can significantly accelerate the calculations of the optical characteristics of clouds. It is ascertained that the optical characteristics are in a good agreement with the lidar observation results throughout the range of sizes calculated even at deformation angles of a few degrees.

Keywords: irregular ice columns, cirrus clouds, physical optics, light scattering, ice crystals
DOI: 10.1134/S1024856017060100

INTRODUCTION

Cirrus clouds are thin semitransparent clouds located at altitudes of 5–12 km and comprising mainly ice particles with sizes from tens to a thousand microns. The study of cirrus clouds has an important applied significance, because they strongly influence the planet radiation balance [1–5]. Present-day numerical models of the weather forecast require on-line information about the cloudiness state on the global scale in order to increase the forecast accuracy [6–8]. Optical characteristics of cirrus clouds significantly depend on microphysical parameters: the form and orientation of ice crystalline particles generating a cloud [9–11]. The main instrument, which allows the on-line acquisition of data on the microphysical parameters of clouds, are lidars [12–14]. However, the interpretation of lidar signals is an intricate problem.

A significant step forward in the solution of the problem of lidar signal interpretation is the method of laser polarization sensing [15–18], developed at Tomsk State University (TSU) and the Institute of Atmospheric Optics (IAO SB RAS). This method allows us to efficiently determine the spatial orientation of plane crystalline particles of cirrus clouds.

The interpretation of the lidar signal requires the solution of the direct problem of the light scattering by particles characteristic of cirrus clouds. The method of physical optics [19, 20] developed at IOA SB RAS and based on the algorithm of tracing optical beams [21–23] provides the solution of this problem. The method allowed us to find the solution for quasi-horizontally oriented ice particles [24, 25], which plays an important part when interpreting scanning lidar data [26]. However, the solution obtained for ideal hexagonal ice columns poorly agrees with data from experimental observations in the case of their chaotic orientation [27–29]. In this work, we present the solution of the problem for irregular hexagonal columns, which agree well with lidar measurements and can be used in their interpretation.

IRREGULAR PARTICLES

Results of numerical solutions of the light scattering problem for ideal hexagonal ice columns differ from the results of experimental observation. Figures 1 and 2 show the lidar (LR) and depolarized (DR) ratios calculated for an ideal ice column depending on the particle size.

In calculations, the following experimentally obtained dependence [30] between the diameter and length of the hexagonal column was used:

$$\begin{cases} D = 0.7L, & L < 100\ \mu\text{m}, \\ D = 0.96\sqrt{L}, & L > 100\ \mu\text{m}, \end{cases} \quad (1)$$

where L is the column length; D is the circle diameter around the hexagonal base.

Since the parameter of the form

$$Q = \frac{L}{D} \quad (2)$$

and the dependence of the diameter on the column length vary with the particle size, it is convenient to use the maximal size of a hexagonal particle in order to determine its characteristic size, equal to

$$D_{\max} = \sqrt{D^2 + L^2}. \quad (3)$$

Since experimentally observable values of the depolarization ratio, lying in range 0.3–0.5, and the lidar ratio, lying in range 20–40, disagree with the calculations, shown in Figs. 1 and 2, throughout most of the range of particle sizes, the conclusion can be drawn that the model of ideal hexagonal particles poorly describes the microphysical content of clouds.

The above-said is supported by the fact that a halo of 46° characteristic of the light scattering on the ideal hexagonal particles [32] (Fig. 3) is seldom observed experimentally as compared to a halo of 22°, which is proved by observations, conducted, for example, at the TomSky chamber [33, 34].

It should be noted that a halo of 22° is formed on lateral sides of a crystal, the angle between which is 60°. A halo of 46° is formed due to an angle of 90° between the base and lateral sides of the crystal (see, for example, [32]). Taking into account the observation results, it is possible to assert that in the overwhelming majority of cases, i.e., in the presence of a halo of 22° at a simultaneous absence of halo of 46°, cirrus clouds consist of hexagonal ice particles with the irregular bases.

Many existing particles have a two-sided angle of 60° at a simultaneous absence of 90° angle. However, it is necessary to take into account the fact that the backscattered light consists of two components, mirror and angular. Both components are described in detail in [25, 27]. In this case, the mirror component is significantly lower than the angular one for ideal hexagonal columns and, as a consequence, the lidar ratio is very small (on the order of 5). The lidar ratio is determined by the formula

$$LR = \frac{2A}{M_{11}}, \quad (4)$$

where $2A$ is the extinction cross section; A is the mean area of the particle projection; M_{11} is the scattering differential cross section, including the angular and mirror components.

For a particle lacking an angle of 90°, the angular component is absent, and the lidar ratio, formed only by the mirror component, is very high, more than several hundreds. In this case, results of lidar observations point to the lidar ratio in the range 20–40, i.e., the angular component is present, but to a lesser degree than for an ideal hexagonal column. The particle with an irregular angle of 90° corresponds to such a descrip-

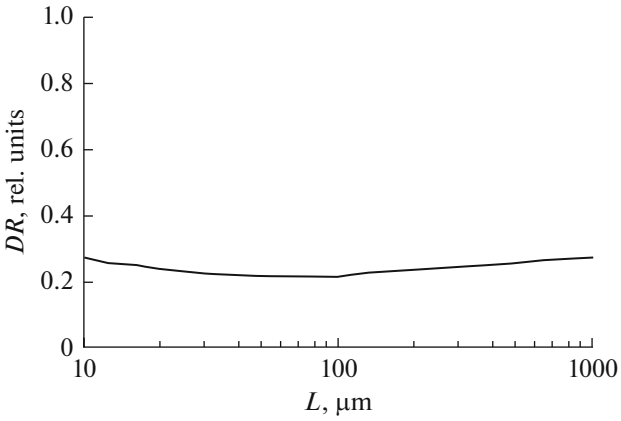

Fig. 1. Depolarization ratio for an ideal hexagonal column in dependence versus its length.

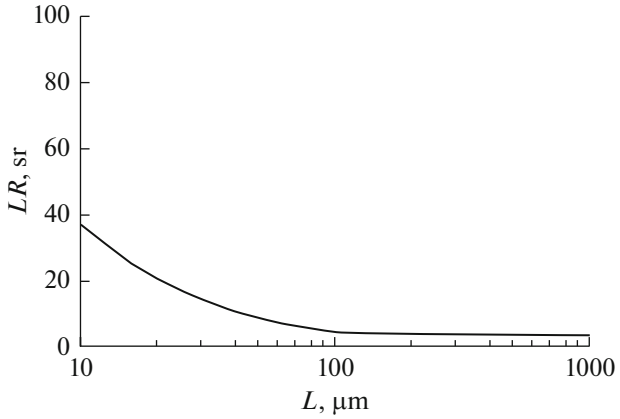

Fig. 2. Lidar ratio for an ideal hexagonal column versus its length.

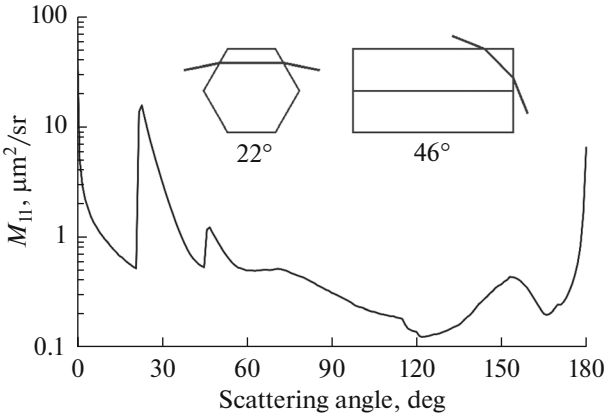

Fig. 3. Differential cross section of the scattering M_{11} for a chaotically oriented hexagonal column of 150 μm in length and 60 μm in diameter at a wavelength of 532 nm.

tion. Thus, a good agreement of theoretical optical characteristics with lidar observation results can be expected for particles with a small angle of irregularity. To test this hypothesis, let us study the optical characteristics of the particles depending on the magnitude of their irregularity. This will help us to improve the accuracy of the available algorithms for lidar signal interpretation.

In order to estimate the influence of the magnitude of irregularity on the optical characteristics, the particle shown in Fig. 4 was used. The irregularity magnitude is determined by the angle ξ, which varies between 0 and 10°. The particle irregularity is selected in such a way as to get rid of the particle symmetry.

In this work, optical characteristics of only chaotically oriented irregular columns are considered, for which the Mueller matrix

$$\mathbf{M} = \frac{1}{8\pi^2}\int_0^{2\pi}\int_0^{2\pi}\int_0^{\pi}\mathbf{M}_f \sin\beta\, d\beta\, d\gamma\, d\alpha, \qquad (5)$$

where $\mathbf{M}_f$ is the Mueller matrix at a fixed orientation; α, β, and γ are Eulerian angles (see Fig. 4).

CALCULATION OF OPTICAL CHARACTERISTICS OF IRREGULAR PARTICLES

Optical characteristics of chaotically oriented convex particle for backscattering are fully determined by the mean area of the particle projection A and Mueller matrix in the form

$$\mathbf{M} = \begin{pmatrix} M_{11} & 0 & 0 & M_{14} \\ 0 & M_{22} & 0 & 0 \\ 0 & 0 & -M_{22} & M_{34} \\ -M_{14} & 0 & -M_{34} & 1-M_{22} \end{pmatrix} = M_{11}\begin{pmatrix} 1 & 0 & 0 & m_{14} \\ 0 & m_{22} & 0 & 0 \\ 0 & 0 & -m_{22} & m_{34} \\ -m_{14} & 0 & -m_{34} & 1-2m_{22} \end{pmatrix}, \qquad (6)$$

where $m_{14} = 0$ for ideal hexagonal particles and <0.05 at irregularity angles up to 10°; therefore, this element can be neglected.

Since of practical interest are lidar (4), depolarization

$$DR = \frac{M_{11} - M_{22}}{M_{11} + M_{22}} \qquad (7)$$

and spectral ratios

$$CR = \frac{M_{11}^{1064}}{M_{11}^{532}}, \qquad (8)$$

it is necessary to calculate only three values: A, M_{11}, and M_{22} for each wavelength. Here indices 1064 and 532 mean the wavelength at which the values are calculated.

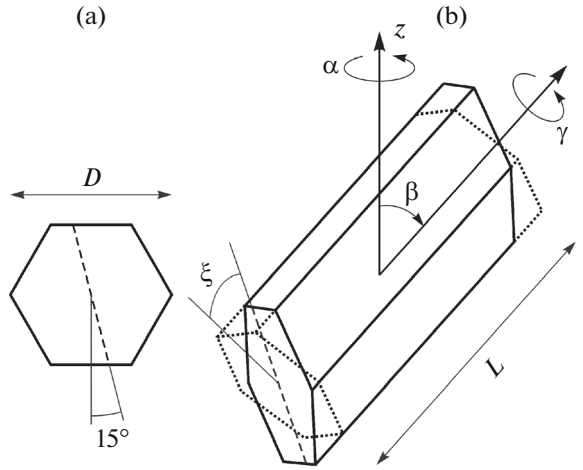

Fig. 4. The model of irregular particle.

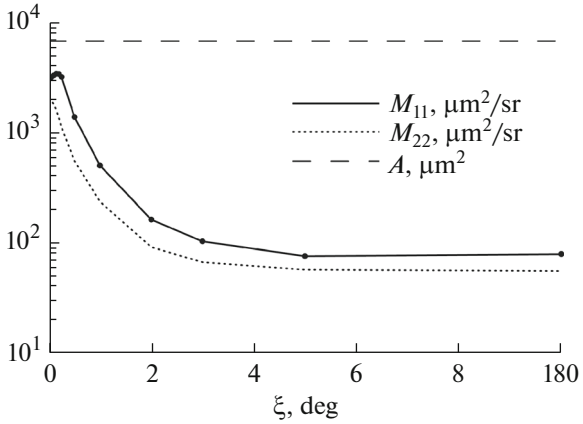

Fig. 5. Dependence of optical characteristics on the angle of the particle irregularity. Points denote the irregular particles selected for the calculation.

Despite the fact that the method of physical optics is significantly faster than accurate methods [35, 36], the calculation of optical properties of the chaotically oriented particle of the size set consumes a long time, because the adequate averaging over orientations requires the preliminary calculation of millions of fixed orientations [36]. Therefore, it is important to determine the minimal necessary number of particles for the calculation, which adequately describes the dependence of optical characteristics on the particle irregularity angle. The example of the dependence of optical characteristics at the 532-nm wavelength on the irregularity angle for 100-μm particle is shown in Fig. 5.

As is seen from Fig. 5, the dependence of the optical characteristics on the irregularity magnitude can be adequately described from the calculation of optical

characteristics for a few correspondingly selected irregular particles.

Figure 5 shows that the elements of the Mueller matrix significantly change with the irregularity magnitude, supporting the fact that a weak deformation of a two-side angle of 90° causes significant variations in optical characteristics of hexagonal ice columns. Note that the deformation of the shape insignificantly affect the mean area A.

Calculation results also have shown that the rate of variation in the optical characteristics grows with the particle size and with a decrease in the wavelength (Fig. 6).

Since the magnitude and form of crystal irregularity are unknown in a natural cloud, we suppose that the angle of deformation of particles obeys the Mises distribution [37]:

$$p(\xi, \xi_{\text{eff}}) = N_p \exp\left(\frac{\cos(\xi)}{\xi_{\text{eff}}^2}\right). \quad (9)$$

Here ξ_{eff} is the effective angle of the crystal irregularity; N_p is the normalizing constant.

Of the practical interest is the dependence of optical characteristics of crystals on the effective irregularity angle, i.e., the values averaged by the formula

$$\mathbf{M}(\xi_{\text{eff}}) = \frac{\int_0^{10^\circ} \mathbf{M}(\xi) p(\xi, \xi_{\text{eff}}) d\xi}{\int_0^{10^\circ} p(\xi, \xi_{\text{eff}}) d\xi}, \quad (10)$$

where the limits of the integration correspond to initial data, and the integral in the denominator is the normalizing constant for the von Mises distribution. Results of averaging for a 100-μm particle are shown in Fig. 7.

EXTRAPOLATION OF CALCULATED DATA

Hexagonal particles observed in cirrus clouds essentially differ in their sizes. The majority of particles have sizes from 10 to 1000 μm [30, 38, 39]; however, very small particles (~5 μm) and very large ones (~10000 μm) can be also observed.

In the case where the cloud of particles is meant, it is supposed for simplicity that the distribution of particle sizes obeys the gamma distribution:

$$\eta(D_{\max}, D_m) = \frac{1}{\Gamma(p) D_m} \left(\frac{D_{\max}}{D_m}\right)^{p-1} \exp\left(-\frac{D_{\max}}{D_m}\right) \quad (11)$$

(D_m is the modal size; $\Gamma(p)$ is the gamma function; and p can be taken as equal to 2 [40]). In this case, the optical characteristics averaged over sizes $\mathbf{M}(D_m)$ can be calculated as

$$\mathbf{M}(D_m) = \int \mathbf{M}(D_{\max}) \eta(D_{\max}, D_m) dD_{\max}, \quad (12)$$

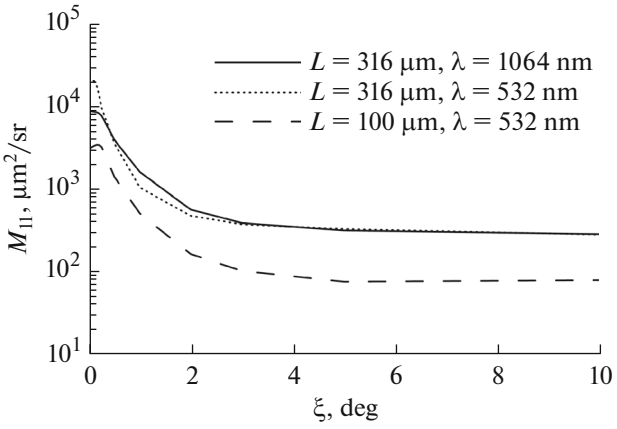

Fig. 6. Dependence of the differential cross section on the angle of irregularity, particle size, and wavelength.

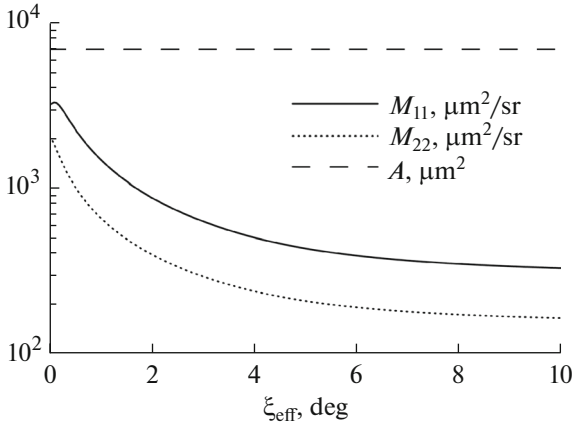

Fig. 7. Dependence of optical characteristics on the effective irregularity angle of the particle at a wavelength of 532 nm.

where the modal size varies between 10 and 1000 μm, and the integral, generally speaking, is taken from 0 to infinity.

In order to conduct the adequate averaging in the above range of modal sizes, it is sufficient to have initial data in the range between at least 5 and 10000 μm, and renormalize the gamma distribution taking into account the limited region of integration:

$$\mathbf{M}(D_m) = \frac{\int_5^{10000} \mathbf{M}(D_{\max}) \eta(D_{\max}, D_m) D_{\max}}{\int_5^{10000} \eta(D_{\max}, D_m) D_{\max}}. \quad (13)$$

Calculation of optical characteristics for particles of fixed sizes was conducted by the method of physical optics [19, 20] in accordance with the technique presented earlier [41].

Table 1

Particle type	Range and ratio of sizes	Wavelength, nm	a	b	c	d	Maximal error, %
Hexagonal column	$D = 0.7L$, $10 < L < 100$	355	2.981	−2.230	3.003	−2.465	0.4
		532	2.942	−2.395	2.994	−2.679	0.6
		1064	2.903	−2.652	2.993	−3.007	1.0
	$D = 6.96L^{0.5}$, $100 \le L < 1000$	355	1.558	0.627	1.491	0.562	0.2
		532	1.542	0.424	1.490	0.337	0.3
		1064	1.530	0.108	1.494	−0.002	0.4
Hexagonal plate	$L = 2.0202D^{0.449}$ $10 < D < 1000$	355	1.884	−0.982	1.875	−1.297	4.4
		532	1.875	−1.213	1.870	−1.493	3.8
		1064	1.869	−1.545	1.869	−1.796	2.5
Bullet	$D = 2.31L^{0.63}$ $10 < L < 1000$	355	1.947	−1.116	1.905	−1.280	1.7
		532	1.917	−1.280	1.893	−1.471	1.6
		1064	1.870	−1.485	1.875	−1.729	2.2
Droxtals	$10 < D < 80$	355	2.247	−1.783	2.198	−2.061	2.1
		532	2.314	−1.915	2.272	−2.222	1.5
		1064	2.616	−2.493	2.536	−2.750	1.8
	$80 \le D < 1000$	355	2.132	−1.595	2.142	−2.011	0.7
		532	2.132	−1.595	2.142	−2.011	0.6
		1064	2.132	−1.595	2.142	−2.011	0.8

Since the computational complexity of the method increases with increasing particle size, it was possible to obtain the optical characteristics in reasonable time only for particles with sizes up to 1000 μm. The bottom boundary of size, 10 μm, was dictated by the limits of applicability of the method of physical optics [42]. The calculation result allowed us to reveal a very important fact: logarithms of the elements M_{11} and M_{22} can be approximated with a good accuracy by linear functions of the size logarithm

$$\log(M_{11}) = a\log(x) + b,$$
$$\log(M_{22}) = c\log(x) + d, \quad (14)$$

where x is equal to the diameter D for plates and droxtals and to the length L for columns and "bullets"; the coefficients a, b, c, and d are given in Table 1.

As an example, Fig. 8 shows calculations and results of interpolation at a wavelength of 532 nm. The interpolation errors are shown in Fig. 9.

The dependence on the optical characteristics A, M_{11}, and M_{22} for an ideal hexagonal column is shown in Fig. 10. It is seen that the variation in dependence of the column length on the diameter at the point of 100 μm in accordance with Eq. (1) leads to a variation in the linear approximation of the parameters.

A possibility of linear approximation of all three necessary parameters allows the extrapolation of the numerical solution for ideal hexagonal columns to the necessary range 5–10000 μm.

Such an extrapolation is possible also for irregular particles. As an example, Fig. 11 shows the dependence of the element M_{11} on the size and value of the irregularity (a wavelength is 532 nm). The calculation was conducted for particles of seven sizes: 10, 31.6, 100, 316, 526, and 1000 μm.

Figures 12 and 13 show linear approximations of optical characteristics for effective angles of irregularities of 3° and 7°. Figures 12 and 13 confirm the possibility of the linear extrapolation for irregular columns as well.

OPTICAL CHARACTERISTICS OF IRREGULAR PARTICLES

Figures 14–17 show the depolarization, lidar, and spectral ratios and differential cross sections of the

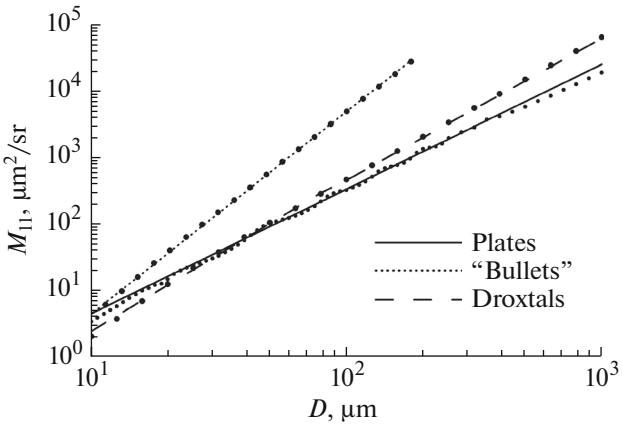

Fig. 8. Differential cross section of scattering M_{11} for plates, "bullets", and droxtals. Values calculated by the method of physical optics are denoted by points.

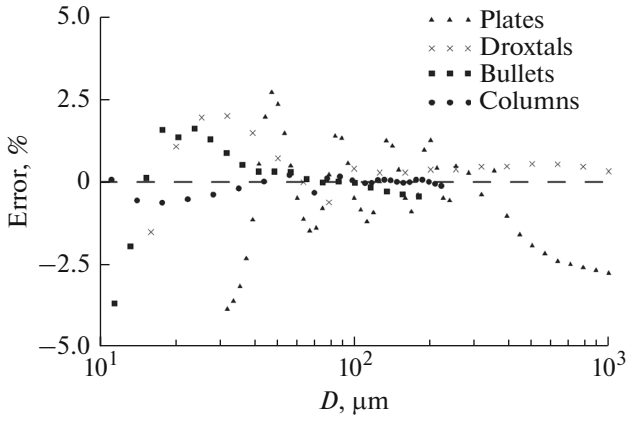

Fig. 9. Interpolation errors versus the particle diameter for a wavelength of 532 nm of the incident light.

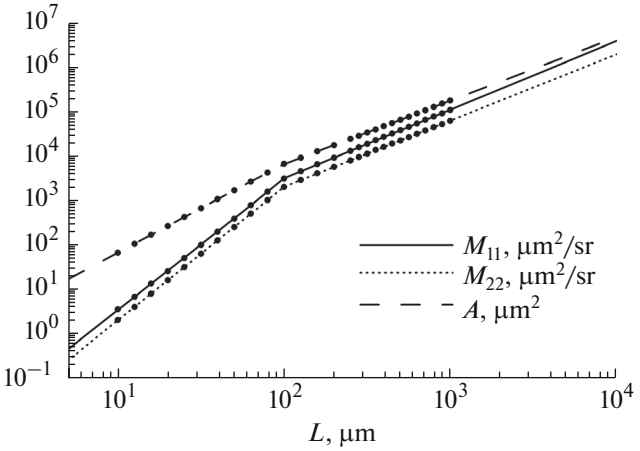

Fig. 10. Size dependence of optical characteristics of an ideal column. Points denote the sizes selected for the calculations.

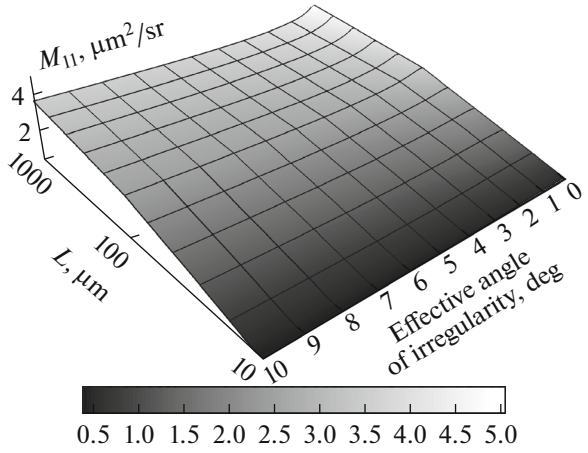

Fig. 11. Dependence of the element M_{11} of the Mueller matrix for an irregular column on the particle size and the effective angle of irregularity.

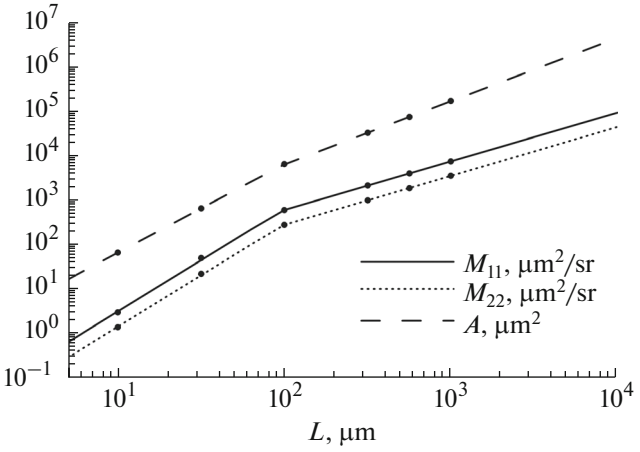

Fig. 12. Size dependence of optical characteristics of an irregular column. The effective angle of irregularity is 3°. Points denote sizes selected for the calculation.

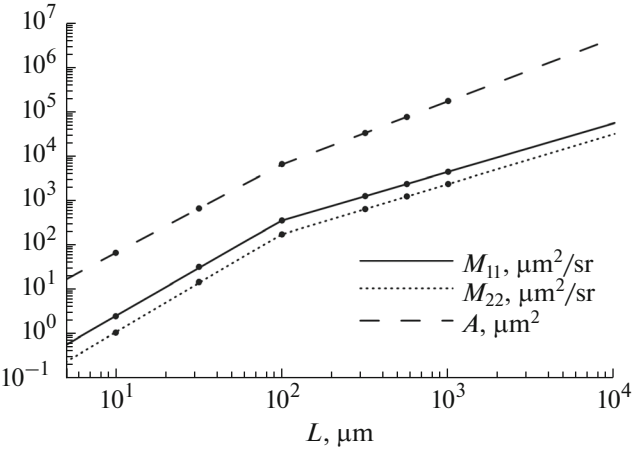

Fig. 13. Size dependence of optical characteristics of an irregular column. The effective angle of irregularity is 7°. Points denote sizes selected for the calculation.

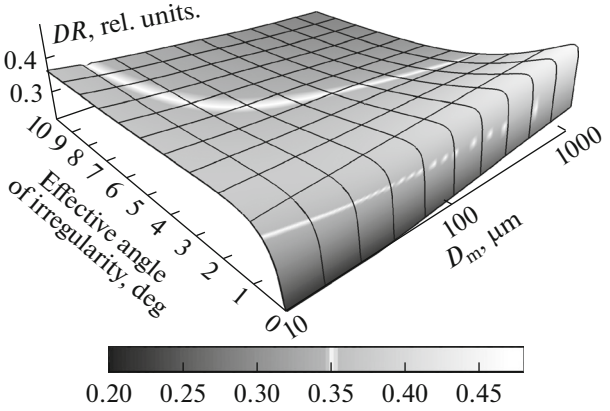

Fig. 14. Depolarization ratio for an irregular column versus the effective angle of irregularity and the modal size (wavelength is 532 nm).

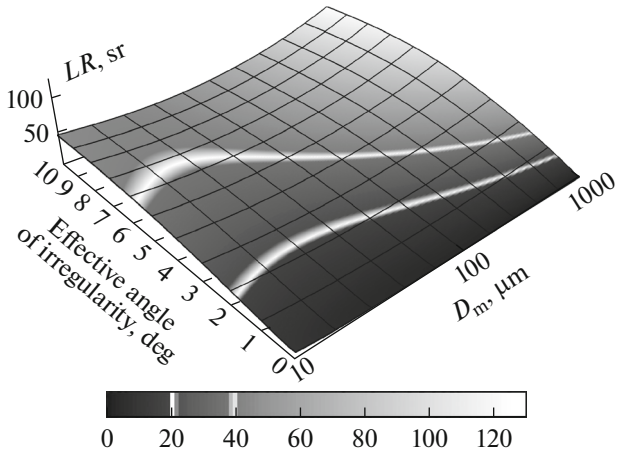

Fig. 15. Lidar ratio for an irregular column versus the effective angle of irregularity and modal size (wavelength is 532 nm).

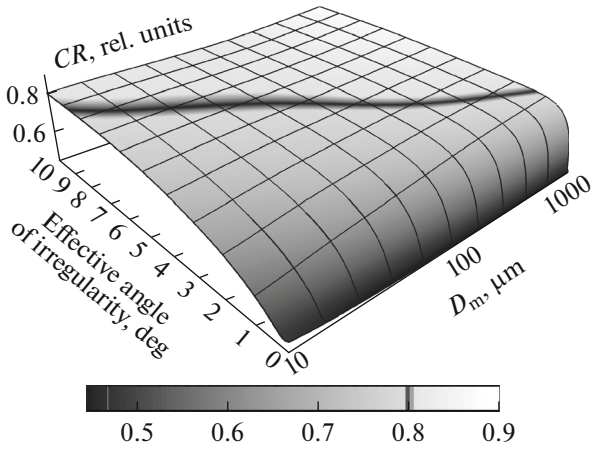

Fig. 16. Spectral ratio for wavelengths 1064/532 nm for the irregular column, depending on the effective angle of irregularity and modal size.

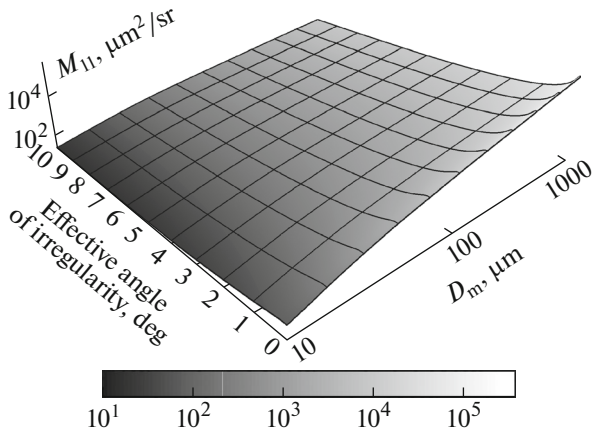

Fig. 17. Differential cross section for an irregular column versus the effective angle of irregularity and modal size (wavelength is 532 nm).

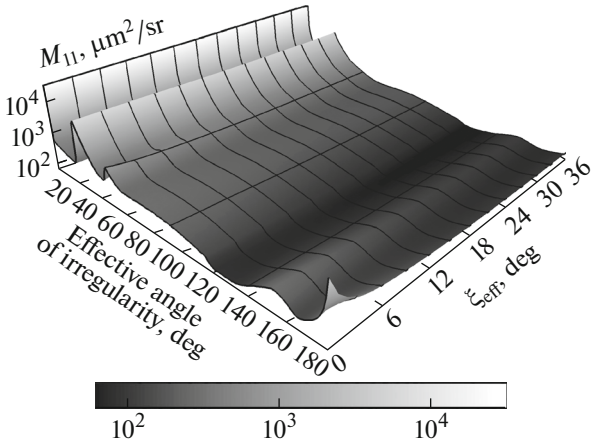

Fig. 18. Differential cross section for an irregular column versus the effective angle of irregularity (wavelength is 532 nm for 100-micron particle).

scattering (M_{11}) for irregular hexagonal columns. Figure 18 shows the differential cross section over all scattering angles versus the irregularity angle calculated in the geometrical optics approximation for a wavelength of 532 nm, which demonstrates the break of a halo of 46° with an increase in the irregularity angle.

CONCLUSIONS

Thus, it is shown in this work that optical characteristics, calculated for irregular particles, agree well with lidar observation results even at small angles of irregularity. In particular, for a cloud of particles with a modal size of 100 μm at an effective irregularity angle of 3°, the calculated values of the depolarization (0.38), lidar (30 sr), and spectral (0.78) ratios reproduce the lidar observation results well [43]. It is also seen that for such a particle a halo of 46° is absent, which corresponds to observations.

The calculation results have shown that the model of irregularity suggested adequately describes optical characteristics of actual cirrus clouds in a wide range of experimental values.

The results of the work can be used for the interpretation of lidar signals, and show the necessity of taking into account weak irregularities of the shape of cirrus clouds when calculating the optical characteristics.

ACKNOWLEDGMENTS

The author is grateful to V. A. Shishko for his help in calculations.

This work was partly supported by the Russian Foundation for Basic Research (grant nos. 15-05-06100

and 16-35-60089) and President of the Russian Federation (grant nos. MK-2495.2017.5 and SS 8199.2016.5).

REFERENCES

1. K. N. Liou, "Influence of Cirrus clouds on weather and climate processes: A global perspective," Mon. Weather. Rev. **114** (6), 1167–1199 (1986).
2. G. L. Stephens, S.-C. Tsay, P. W. Stackhouse, Jr., and P. J. Flatau, "The relevance of the microphysical and radiative properties of cirrus clouds to climate and climatic feedback," J. Atmos. Sci. **47** (14), 1742–1754 (1990).
3. A. J. Baran, "From the single-scattering properties of ice crystals to climate prediction: A way forward," Atmos. Res. **112**, 45–69 (2012).
4. P. Wendling, R. Wendling, and H. K. Weickmann, "Scattering of solar radiation by hexagonal ice crystals," Appl. Opt. **18** (15), 2663–2671 (1979).
5. K. Sassen and S. Benson, "A midlatitude cirrus cloud climatology from the facility for atmospheric remote sensing: II. Microphysical properties derived from lidar depolarization," J. Atmos. Sci. **58** (15), 2103–2112 (2001).
6. V. A. Kuz'min and A. V. Dikinis, "Integrated use of remote sensing and ground-based observation data and numerical weather forecasts in automated runoff forecasting," Uchen. Zapiski Ros. Gos. Gidrometeorol. Univ. **22** (22), 16–27 (2011).
7. S. A. Soldatenko, A. V. Tertyshnikov, and N. V. Shirshov, "The impact estimate of satellite information on the quality of numerical weather prediction," Sovr. Probl. Distantsionnogo Zondirovaniya Zemli Kosmosa **12** (4), 38–47 (2015).
8. E. Kalnay, *Atmospheric Modeling, Data Assimilation and Predictability* (University Press, Cambridge, 2002).
9. A. J. Baran, "A review of the light scattering properties of cirrus," J. Quant. Spectrosc. Radiat. Transfer **110** (14–16), 1239–1260 (2009).
10. Y. Takano and K. N. Liou, "Solar radiative transfer in cirrus clouds. Part I. Single scattering and optical properties of hexagonal ice crystals," J. Atmos. Sci. **46** (1), 3–19 (1989).
11. A. Borovoi, A. Konoshonkin, and N. Kustova, "Backscatter ratios for arbitrary oriented hexagonal ice crystals of cirrus clouds," Opt. Lett. **39** (19), 5788–5791 (2014).
12. I. V. Samokhvalov, I. D. Bryukhanov, S. V. Nasonov, I. V. Zhivotenyuk, and A. P. Stykon, "Investigation of the optical characteristics of cirrus clouds with anomalous backscatterring," Rus. Phys. J. **55** (8), 925–929 (2013).
13. K. Sassen, V. K. Kayetha, and J. Zhu, "Ice cloud depolarization for nadir and off-nadir CALIPSO measurements," Geophys. Rev. Lett. **39** (20), L20805 (2012). doi 10.1029/2012GL053116
14. I. V. Samokhvalov, S. M. Bobrovnikov, P. P. Geiko, A. V. El'nikov, and B. V. Kaul', "Development of Tomsk State University lidar as a unique complex for atmospheric monitoring," Atmos. Ocean. Opt. **19** (11), 895–898 (2006).
15. B. V. Kaul', Doctoral Dissertation in Mathematics and Physics (Institute of Atmospheric Optics SB RAS, Tomsk, 2004).
16. B. V. Kaul', S. N. Volkov, and I. V. Samokhvalov, "Studies of ice crystal clouds through lidar measurements of backscattering matrices," Atmos. Okean. Opt. **16** (4), 325–332 (2003).
17. D. N. Romashov, B. V. Kaul', and I. V. Samokhvalov, "Data bank for interpreting results of polarization sensing of crystalline clouds," Atmos. Okean. Opt. **13** (9), 794–800 (2000).
18. I. V. Samokhvalov, S. V. Nasonov, I. D. Bryukhanov, A. G. Borovoi, B. V. Kaul', N. V. Kustova, and A. V. Konoshonkin, "The analysis of the backscattering matrix for cirrus clouds with anomalous backscattering," Izv. Vyssh. Ucheb. Zaved., Fiz. **56** (8/3), 281–283 (2013).
19. A. V. Konoshonkin, N. V. Kustova, V. A. Osipov, A. G. Borovoi, K. Masuda, H. Ishimoto, and H. Okamoto, "Physical optics approximation for solving problems of light scattering on the ice crystal particles: Comparison of the vector formulations of diffraction," Opt. Atmos. Okeana **28** (9), 830–843 (2015).
20. A. Borovoi, A. Konoshonkin, and N. Kustova, "The physics-optics approximation and its application to light backscattering by hexagonal ice crystals," J. Quant. Spectrosc. Radiat. Transfer **146**, 181–189 (2014).
21. A. V. Konoshonkin, N. V. Kustova, and A. G. Borovoi, "Beam splitting algorithm for the problem of light scattering by atmospheric ice crystals. Part 1. Theoretical foundations of the algorithm," Atmos. Ocean. Opt. **28** (5), 441–447 (2015).
22. A. V. Konoshonkin, N. V. Kustova, and A. G. Borovoi, "Beam splitting algorithm for the problem of light scattering by atmospheric ice crystals. Part 2. Comparison with the ray tracing algorithm," Atmos. Ocean. Opt. **28** (5), 448–454 (2015).
23. A. Konoshonkin, N. Kustova, and A. Borovoi, "Beam-splitting code for light scattering by ice crystal particles within geometric-optics approximation," J. Quant. Spectrosc. Radiat. Transfer **164**, 175–183 (2015).
24. A. Borovoi, Y. Balin, G. Kokhanenko, I. Penner, A. Konoshonkin, and N. Kustova, "Layers of quasi-horizontally oriented ice crystals in cirrus clouds observed by a two-wavelength polarization lidar," Opt. Express **22** (20), 24566–24573 (2014).
25. A. Borovoi, A. Konoshonkin, N. Kustova, and H. Okamoto, "Backscattering Mueller matrix for quasihorizontally oriented ice plates of cirrus clouds: Application to CALIPSO signals," Opt. Express **20** (27), 28222–28233 (2012).
26. A. V. Konoshonkin, "Simulation of the scanning lidar signals for a cloud of monodisperse quasi-horizontal oriented particles," Opt. Atmos. Okeana **29** (12), 1053–1060 (2016).
27. A. Borovoi, N. Kustova, and A. Konoshonkin, "Interference phenomena at backscattering by ice crystals of cirrus clouds," Opt. Express **23** (19), 24557–24571 (2015).
28. H. M. Cho, P. Yang, G. W. Kattawar, S. L. Nasiri, Y. Hu, P. Minnis, C. Trepte, and D. Winker, "Depolar-

ization ratio and attenuated backscatter for nine cloud types: Analyses based on collocated CALIPSO lidar and MODIS measurements," Opt. Express **16** (6), 3931–3948 (2014).

29. R. Yoshida, H. Okamoto, Y. Hagihara, and H. Ishimoto, "Global analysis of cloud phase and ice crystal orientation from Cloud-Aerosol Lidar and Infrared Pathfinder Satellite Observation (CALIPSO) data using attenuated backscattering and depolarization ratio," J. Geophys. Res. **115** (32), D00 (2010). doi 10.1029/2009JD012334
30. D. L. Mitchell and W. P. Arnott, "A model predicting the evolution of ice particle size spectra and radiative properties of cirrus clouds. Part II: Dependence of absorption and extinction on ice crystal morphology," J. Atmos. Sci. **51** (6), 817–832 (1994).
31. V. Wolf, J. Reichardt, U. Gorsdorf, A. Reigert, R. Leinweber, and V. Lehmann, "Synergy between ground-based remote sensing systems in microphysical analysis of cirrus clouds," Proc. SPIE—Int. Soc. Opt. Eng. **9246**, 92460K (2014). doi 10.1117/12.2065674
32. O. A. Volkovitskii, L. N. Pavlova, and A. G. Petrushin, *Optical Properties of Crystalline Clouds* (Gidrometeoizdat, Leningrad, 1984) [in Russian].
33. http://sky.iao.ru/
34. A. M. Morozov, V. P. Galileiskii, A. I. Elizarov, and D. V. Kokarev, "Observation of the mirror reflection of lighted underlying surface by a cloudy layer of ice plates," Opt. Atmos. Okeana **30** (1), 88–92 (2017).
35. A. V. Konoshonkin, N. V. Kustova, A. G. Borovoi, Y. Grynko, and J. Forstner, "Light scattering by ice crystals of cirrus clouds: Comparison of the physical optics methods," J. Quant. Spectrosc. Radiat. Transfer **182**, 12–23 (2015).
36. A. V. Konoshonkin, A. G. Borovoi, N. V. Kustova, H. Okamoto, H. Ishimoto, Y. Grynko, and J. Forstner, "Light scattering by ice crystals of cirrus clouds: From exact numerical methods to physical-optics approximation," J. Quant. Spectrosc. Radiat. Transfer (2017). doi 10.1016/j.jqsrt.2016.12.024
37. K. V. Mardia, *Statistics of Directional Data* (Academic, New York, 1972).
38. D. L. Mitchell, "A model predicting the evolution of ice particle size spectra and radiative properties of cirrus clouds. Part 1. Microphysics," J. Atmos. Sci. **51** (6), 797–816 (1994).
39. A. H. Auer and D. L. Veal, "The dimension of ice crystals in natural clouds," J. Atmos. Sci. **27** (6), 919–926 (1970).
40. K. Sato and H. Okamoto, "Characterization of Ze and LDR of non-spherical and inhomogeneous ice particles for 95-ghz cloud radar: Its application to microphysical retrievals," J. Geophys. Res., D **111**, 22213 (2006).
41. A. V. Konoshonkin, N. V. Kustova, V. A. Shishko, and A. G. Borovoi, "The technique for salving the problem of light backscattering by ice crystals of cirrus clouds by the physical optics method for a lidar with zenith scanning," Atmos. Ocean. Opt. **29** (3), 252–262 (2016).
42. A. Borovoi, A. Konoshonkin, and N. Kustova, "Backscattering reciprocity for large particles," Opt. Lett. **38** (9), 1485–1487 (2013).
43. Z. Wang, A. Borovoi, D. Liu, Z. Tao, C. Ji, C. Xie, B. Wang, Z. Zhong, and Y. Wang, "Properties of cirrus cloud by a three wavelength Raman Mie polarization lidar: Observation and model match," Proc. SPIE—Int. Soc. Opt. Eng. **10035**, 100352 (2016).

Translated by S. Ponomareva